Dalton Transactions

ROYAL SOCIETY OF CHEMISTRY

PAPER

View Article Online
View Journal | View Issue

Check for updates

Cite this: *Dalton Trans.*, 2024, **53**, 7197

Spin crossover in {Fe(pyrazine)[M(CN)$_4$]} (M = Ni, Pt) thin films assembled on fused silica substrates†

Fayan Lai, Gábor Molnár, * Saioa Cobo* and Azzedine Bousseksou*

Received 16th February 2024,
Accepted 30th March 2024

DOI: 10.1039/d4dt00454j

rsc.li/dalton

Thin films with thicknesses in the range between *ca.* 10–50 nm of the spin crossover (SCO) compound {Fe(pyrazine)[μ_4-M(CN)$_4$]} (M = Ni, Pt) have been deposited on fused silica substrates using a sequential assembly method and 4-pyridinecarboxylic acid as anchoring layer. Film morphology and crystallinity were assessed by means of atomic force microscopy and grazing incidence X-ray diffraction, respectively. The intensity of the π–π^* transition of the pyrazine ligand at 270 nm, being rather insensitive to the spin state of the complex, was used to follow the film growth as a function of different deposition parameters. On the other hand, the spin state changes were inferred from the temperature dependence of absorption bands appearing at 540, 490 and 310 nm in the low spin state. In line with their amorphous nature, each film displays a very gradual thermal spin crossover between *ca.* 100–300 K, independently of its thickness and deposition conditions. These results are not only interesting to better understand the effects of size reduction and organization on the SCO phenomenon, but the deposition of these SCO compounds on electrically insulating and/or optically transparent oxide surfaces opens also the door for various photonic or electronic applications.

1. Introduction

Metal–organic frameworks (MOFs) have attracted considerable attention owing to their vast structural diversity and functional tunability allowing their implementation in a great variety of applications (sensors, catalyst...).[1,2] MOFs are two- or three-dimensional (2D or 3D) coordination networks in which the metals and the organic ligands are linked through a coordination bond to build up an extended network. The choice of these two building blocks conditions the properties of the final architecture.

Among the functional MOFs, Hofmann-type metal–organic frameworks (HtMOF) incorporating spin-crossover (SCO) moieties stand as an appealing subclass.[3–5] These compounds undergo a thermal,[6] piezo,[7] photo[8] or chemo[9] triggered conversion between their high-spin (HS) and low-spin (LS) states leading to spectacular changes of physical properties. The structure of these SCO HtMOFs consists of 2D Fe(II)–cyanide–metal sheets, wherein the coordination sphere of the ferrous ion is completed by a monodentate or bidentate organic ligand. Among the different HtMOFs, those containing pyridine (py) and pyrazine (pz) ligands[6,10,11] stand as the most appealing for building 2D and 3D networks, respectively (Scheme 1).

Since several years, considerable research efforts have been devoted to the deposition of these SCO MOFs on surfaces, in order to facilitate their technological applications.[13–15] Among the different techniques of thin film fabrication, the multilayer sequential assembly (MSA) approach appears particularly promising.[16] In 2006, we reported the successful assembly of thin films of the 3D MOFs {Fe(pz)[μ_4-M(CN)$_4$]} **1** (M = Ni, Pd, Pt) displaying near room temperature SCO.[17] Later we extended this approach to other compounds of this family containing azopyridine[18] and bis(4-pyridyl)acetylene[19] linkers (instead of pyrazine), worked on the surface functionalization[20] and the micro/nanopatterning of the films by lithography methods.[21,22] Finally, by combining these advances, a fully-fledged gas sensor device, based on micro-patterned {Fe(bis(4-pyridyl)acetylene)[μ_4-Pt(CN)$_4$]} films, was developed, allowing the detection of low atmospheric concentrations of volatile organic compounds by means optical diffraction.[23] As an important step, the group of Kitagawa has shown by means of synchrotron X-ray diffraction (XRD) measurements that the {Fe(pz)[μ_4-Pt(CN)$_4$]} films exhibit crystalline order both perpendicular and parallel to the substrate surface.[24] Later, the same group has successfully extended the MSA approach to the assembly of the 2D SCO MOFs {Fe(py)$_2$[μ_4-M(CN)$_4$]} (M = Ni, Pd, Pt)[12,25] and investigated the effects of substrate morphology,[26] film thickness[27] and interfacial strain[28] on the SCO properties. On the other hand, researchers from the University

LCC, CNRS and Université de Toulouse (UPS, INP), Toulouse, France.
E-mail: gabor.molnar@lcc-toulouse.fr, saioa.cobo@lcc-toulouse.fr, azzedine.bousseksou@lcc-toulouse.fr

† Electronic supplementary information (ESI) available. See DOI: https://doi.org/10.1039/d4dt00454j

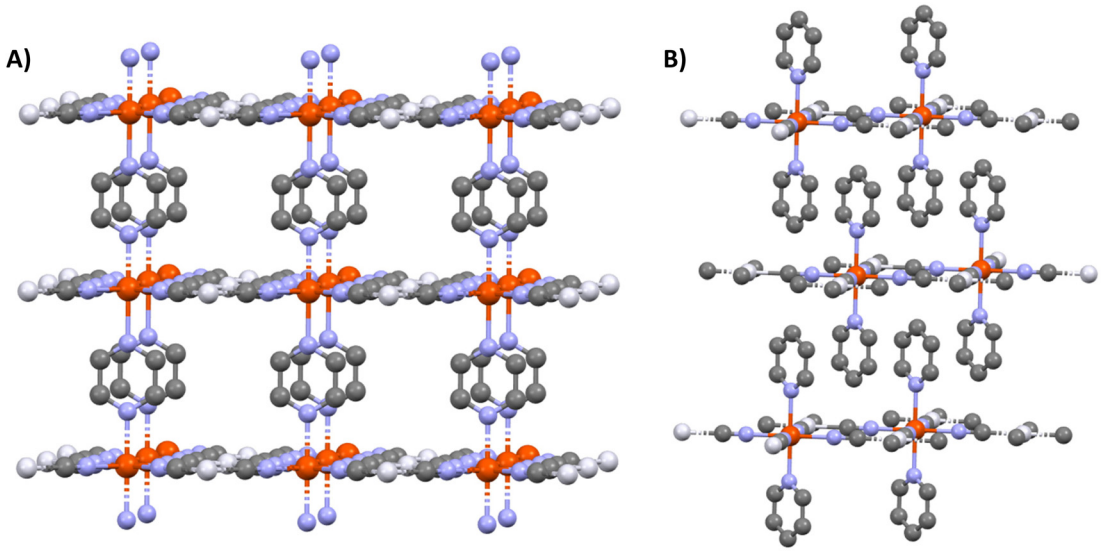

Scheme 1 Schematic structures of $\{Fe(pz)[\mu_4\text{-}M(CN)_4]\}$[11] (A) and $\{Fe(py)_2[\mu_4\text{-}M(CN)_4]\}$[12] (B).

of Valencia focused on the fabrication of ultrathin films of the compound $\{Fe(py)_2[\mu_4\text{-}Pt(CN)_4]\}$,[29] the replacement of pyridine by pyrimidine and isoquinoline ligands,[30] the investigation of the charge transport properties of these films[31] and on the assembly of $\{Fe(py)_2[\mu_4\text{-}Pt(CN)_4]\}/MoS_2$ heterostructures.[32]

Importantly, with the exception of the work in ref. 32, the SCO MOF films were always assembled on gold substrates, which were pre-functionalized with a self-assembled monolayer (SAM) of a pyridine derivative (mercaptopyridine, 4,4′-azopyridine or ethyl-(4-pyridyl)disulfide) in order to achieve high structural and morphological quality of the SCO MOF film. However, if gold affords high quality SAMs, based on thiol derivatives, it cannot be used in certain circumstances. In particular, it appears interesting to assemble SCO MOF films on electrically insulating and/or optically transparent surfaces, which can be mandatory for numerous photonic and electronic applications. In this context, oxides, such as glass, quartz or ITO, are particularly appealing because most of them share the potential for surface functionalization through the reactivity of surface –OH groups as anchoring sites for silanes, phosphonic acid, phosphonates and carboxylic acid derivatives among others.[33] Based on these motivations, in this paper, we report on the elaboration of thin films of $\{Fe(pz)[\mu_4\text{-}M(CN)_4]\}$ (M = Ni, Pt) on fused silica (FS) substrates using 4-pyridinecarboxylic acid as anchoring layer. Taking immediate advantage of the excellent transparency of this substrate in the UV-visible spectral range, we could monitor the film growth and SCO phenomena in a straightforward manner using a simple spectrophotometry setup.

2. Materials and methods

All reagents were of commercial grade and used without further purification. Tetra-*n*-butylammonium tetracyanometalate salts, $\{(TBA)_2M(CN)_4\}$ (M = Ni, Pt) (see Fig. S1 and S2†) were synthetized according to previously described procedures.[34] Rectangular (10 × 10 × 0.5 mm^3), double side polished, UV grade, FS substrates were purchased from MicroChemicals. The substrates were first sonicated successively for 15 min in ethanol, acetone and then washed with deionized water. After drying by an argon flow, the substrates were dipped into a 1 mM ethanolic solution of 4-pyridinecarboxylic acid at room temperature and kept in the solution for 24 h in order to promote the formation of a densely packed SAM. The substrates were then rinsed with ethanol to remove the non-anchored molecules and finally dried in argon flow. During the dipping period, the surface hydroxyl groups of the substrates react with the carboxylic counterpart of the ad-layer in order to form ester groups on the surface. The pre-functionalized FS surfaces were then dipped for 1 min alternatively in $Fe(BF_4)_2{\cdot}6H_2O$, $\{(TBA)_2[M(CN)_4]\}$ and pyrazine solutions (in ethanol) of different concentrations (between 25 and 100 mM). Between each dipping step, the functionalized surface was carefully rinsed with ethanol for 30 s. The dipping and rinsing steps were performed at controlled temperatures (between 213 and 293 K). Finally, the multilayer thin films were dehydrated by heating at 433 K for 30 min in air.

UV-visible transmission spectra of the films were recorded between 200–800 nm using a Cary 60 (Agilent) spectrophotometer. For variable temperature measurements, we used a flow-type liquid nitrogen cryostat equipped with FS windows. The temperature was varied between 300 and 100 K with steps of 10 K both in cooling and in heating modes. Raman spectra were collected using an Xplora (Horiba) Raman micro-spectrometer equipped with a diode laser (785 nm, 0.1 mW). The laser beam was focused on the sample by a ×50 objective (numerical aperture = 0.5), which was also used to collect the scattered photons. FTIR spectra were recorded on a Frontier FTIR instrument (Perkin Elmer) in a range of 4000 to

600 cm^{-1}, either in transmission (films) or ATR (powder) modes. Energy Dispersive X-ray (EDX) analysis were carried out by means of a SEM-FEG JSM 7800F Prime-EDS instrument (Jeol).

The surface topography of the samples was assessed by means of atomic force microscopy (AFM) under ambient air in amplitude-modulation mode using a SmartSPM (Horiba) and HQ: NSC15/Al BS cantilevers (Micromash) with a nominal spring constant of 0.18 N m^{-1} and tip radius of <30 nm. For thickness measurements, the films were locally scratched with a blade and the thickness was established from height distribution histograms covering both scratched and unscratched areas. XRD analyses have been performed on a theta/theta Rigaku Smartlab diffractometer equipped with a D-Tex Ultra 250 linear detector, a regular Cu X-rays tube and a cross-beam optics. The XRD analyses have been performed with the parallel incident beam, at room temperature, with a 2theta range of 8–80°, a step of 0.02°, a counting time of 0.5° min^{-1}, and a grazing incident angle of 0.5°.

3. Results and discussion

The functionalization of the FS surface has been performed using 4-pyridinecarboxylic acid. Modification of surfaces by carboxylic acids are among the most studied ones because these molecules are able to bind to a great variety of oxide surfaces. The binding mode will be dependent on the type of surface oxide, but in the case of the absorption on silica, silyl ester linkages have been detected and reported in the literature.[33,35] The film growth of the complexes {Fe(pz)[μ_4-Ni(CN)$_4$]} (**1-Ni**) and {Fe(pz)[μ_4-Pt(CN)$_4$]} (**1-Pt**) was then achieved *via* stepwise coordination reactions on the surface of the three building blocks, iron(II) cation, pyrazine and the tetracyanometalate anion, $[M(CN)_4]^{2-}$, through the alternate dipping of the pre-functionalized FS substrate into their ethanolic solutions (Scheme 2). This strategy allows a direct control of the film thickness by varying the number (N) of dipping cycles. The two other experimental parameters, which allow the control of the film thickness and film quality, are the concentration of the reactants (c) and the reaction temperature (T).

The growth of the 3D coordination polymer of **1-Ni** on the FS surface was evidenced by UV-visible absorption spectroscopy. Fig. 1A presents the UV-visible absorption spectra of films of **1-Ni** recorded at room temperature during the construction of successive assemblies (from 4 to 20 deposition cycles) at a concentration of the reactants of 50 mM kept at 253 K. The absorption spectra of the films exhibit a dominant absorption band near 270 nm related to π–π* transitions of the pyrazine ligand. As shown in the inset of the Fig. 1A, the absorbance of this band grows almost linearly with the number of deposition cycles showing that the stepwise coordination of **1-Ni** units occurs in a regular manner. By establishing a correlation between the films thickness and the absorbance value one can directly use the spectrophotometer to follow the film thickness changes. To this aim, a thickness analysis was carried out by means of AFM (see Fig. S3–S7†) on the same series of films revealing also a proportionality between the film thickness and the number of deposition cycles (Fig. 1B).

By combining the data from Fig. 1A and B, the absorption coefficient of the film at 270 nm can be estimated as 1.0×10^4 cm^{-1} (see also Fig. S8†). We shall note that the intensity of this absorption band is only weakly altered by the spin state of the film (*vide infra*), hence it appears as a reliable measure of the film thickness even if its actual spin state is not known. It is interesting to notice also that the thickness of the film in these experimental conditions increases by 2.4 ± 0.3 nm for each deposition cycle. This value can be compared with the

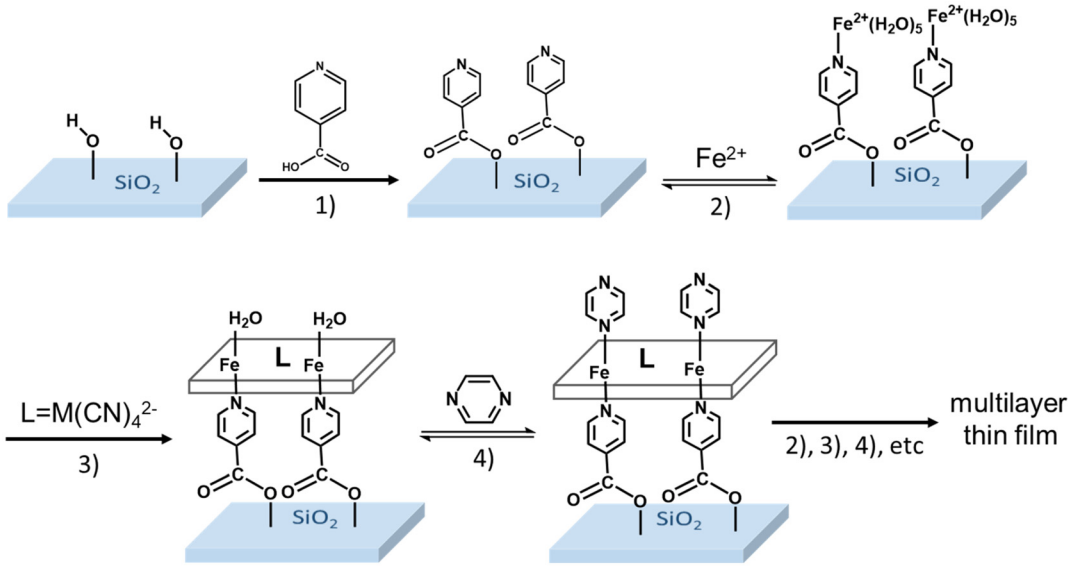

Scheme 2 Sequential assembly of **1-Ni** on a FS surface.

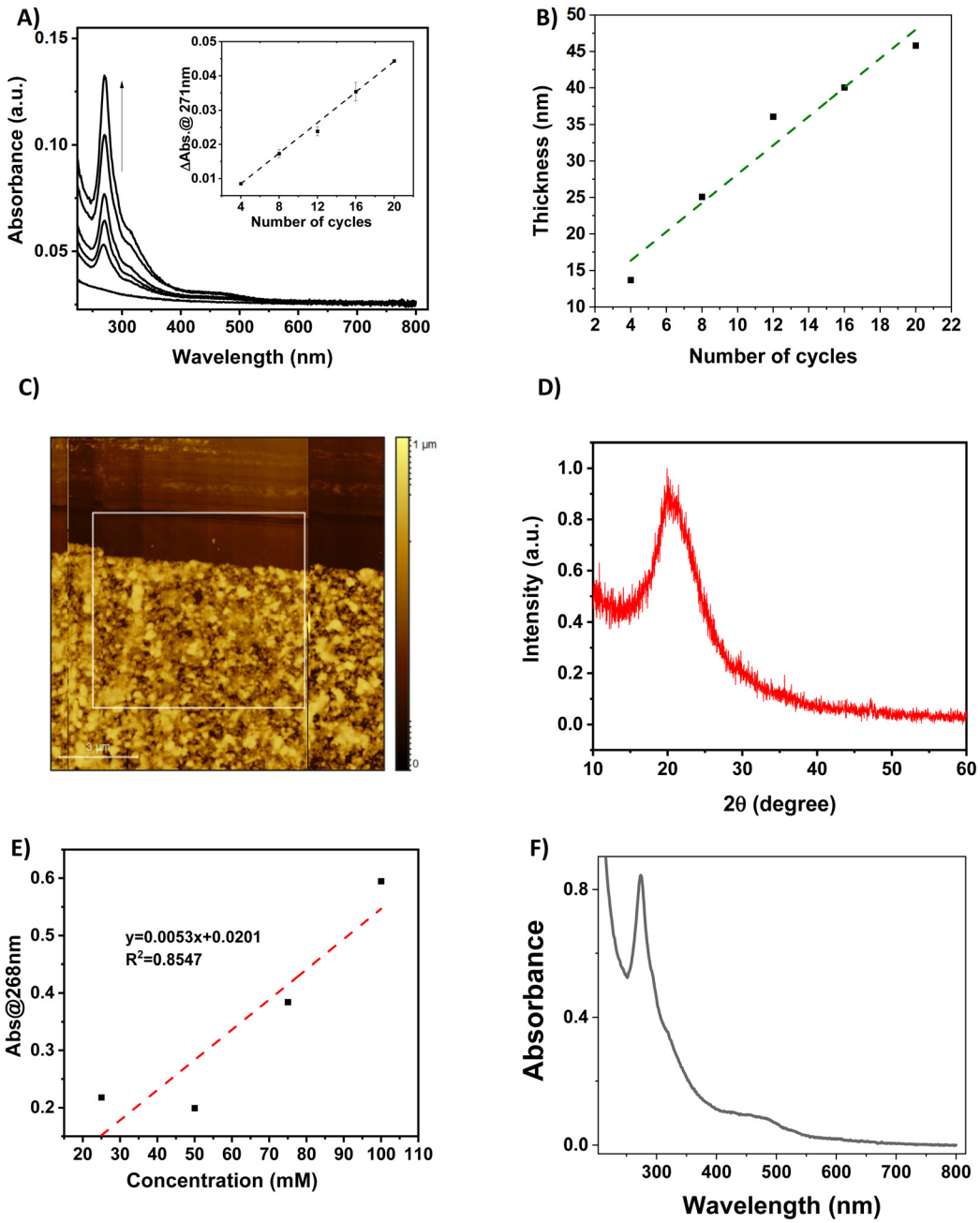

Fig. 1 (A) UV–visible absorption spectra of a film of **1-Ni** recorded during its stepwise growth through 20 deposition cycles (T = 253 K, c = 50 mM). The inset shows the absorbance of the film at 271 nm as a function of the number of deposition cycles. (B) Evolution of the mean thickness of the film **1-Ni** as a function of the number of deposition cycles. (C) Representative AFM surface topography image of a film of **1-Ni** for N = 16 cycles. (The scratch seen in the top of the image was made for film thickness measurement.) (D) Representative XRD pattern of a film of **1-Ni** for N = 16 cycles. (E) Variation of the absorbance of **1-Ni** as a function of the solution concentrations (T = 213 K, N = 16 cycles). (F) UV-vis spectrum of **1-Ni** deposited at room temperature (c = 50 mM, N = 50 cycles).

unit cell dimension of **1-Ni** (*ca.* 0.7 nm),[36] providing a first indication that the film growth does not occur layer-by-layer. Most likely, the SAM formed by the 4-pyridinecarboxylic acid does not afford for an epitaxial growth of the film, leading to different growth directions and ultimately to an enhanced deposition rate. In addition, we employed only one rinsing step between the deposition steps, which might account for the formation of some precipitates. The AFM topography analysis of the different samples allows also appreciating the film morphologies. A typical example is shown in Fig. 1C revealing a densely packed film (16 deposition cycles), with a rather high degree of roughness and ill-defined surface morphology (see also Fig. S3–S7†). The latter finding provides a first hint for the low crystallinity of the films, which was definitely confirmed

by XRD measurements, revealing only a very broad, amorphous signal (see an example in Fig. 1D). The amorphous nature of the thin film contrasts with the highly ordered nature of the thin film on gold surfaces. The most probable hypothesis for this amorphous nature is the disordered growth of the layers, attributed to the misorientation of the anchoring 4-pyridine carboxylic acid with respect to the surface. This phenomenon has been already observed in thin films where carboxylic acid is used as a mediator for a self-assembly. In such cases, the X-ray analysis shows a decrease of the diffraction peaks of the final compound due to the esterification reaction that destroys the crystalline nature of the compounds and forms an entangled chain of amorphous structure.[37]

In order to confirm the structure of the deposited thin films, EDX analyses, Raman and IR spectroscopies were performed on a relatively thick sample (N = 50). EDX spectra (Fig. S9†) show the presence of nickel and iron atoms in a ratio of *ca*. 1.06 at different areas of the film, which is in reasonable agreement with the theoretical value of 1.05. Raman and infrared spectra were recorded at room temperature and compared to the powder spectra (see Fig. S10 and S11†). In both cases, a good match between the vibrational frequencies of the powder and the thin film can be observed. These analyses corroborate thus the proposed chemical structure of the deposited thin films.

The deposition of the films has been also studied as a function of the solution concentrations (25, 50, 75 and 100 mM) for 16 deposition cycles at 213 K (see Fig. S12†). As shown in Fig. 1E, the increase of the solution concentrations leads globally to an increase of the film absorbance, but in a non-linear manner. In addition, the increase of the reaction temperature, while keeping the solution concentrations at 50 mM and the number of cycles at 50 has been investigated. Somewhat surprisingly, we notice that the film deposition can be also performed at room temperature with reasonable efficiency (Fig. 1F). At a first glance, this conclusion seems to contradict previously published papers, in which the kinetics of ligand exchange has been presented as a crucial factor to successfully perform the film deposition at very low temperature.[16,17] However, one shall remind that the film growth mechanisms are certainly rather different, which is also reflected by the observed high roughness of the films obtained in the present case.

The SCO phenomenon in a powdered sample of **1-Ni** is accompanied by a clear colour change from bright yellow at room temperature (HS state), to a deep red colour when cooling (LS state). This thermochromism can be easily monitored by temperature-dependent UV-VIS absorption measurements. It should be noted that the thickness and microstructure of the thin film could have an influence on the SCO phenomena as already reported in the case of various SCO nano-objects.[15] From a theoretical point of view, these size reduction effects can be linked to the increase of the surface-to-volume ratio and the associated gain in importance of the surface free energy over the bulk free energy.[38] One shall also note that other parameters (crystallinity, microstructure, ...) may also play an important role as they can depend on size and/or synthesis conditions.

Because of the excellent transparency of the FS surfaces in the 200–800 nm window, we have been able to follow the spin state change of the deposited 3D metallopolymer films with different thicknesses by monitoring the evolution of their UV-visible spectra during thermal cycles between 300 K and 100 K. As shown in Fig. 2, during the cooling processes, one can observe the emergence of a set of bands in the visible region at *ca*. 490 and 540 nm concomitantly with the intensity increase of the shoulder near 310 nm in the UV. These changes, corresponding to the HS → LS transition, agree with the colour change (yellow → red) at the spin transition already observed for powder samples. Since the spectral changes could be detected in each sample, even for the lowest thickness, these measurements provide a simple means to investigate possible size reduction effects. The deposition of the films has been also studied as a function of the solution concentrations (25, 50, 75 and 100 mM) for 16 deposition cycles at 213 K (see Fig. S12†). Fig. 3 shows the temperature dependence of the absorbance intensity in the heating and cooling modes for films of **1-Ni** deposited using different reactant concentrations (T = 213 K and N = 16). Fig. S13† shows the temperature dependence of the absorbance intensity in the heating and cooling modes as function of the number of dipping cycles (T = 213 K and c = 50 mM). The first important observation is that the SCO is very gradual (spans between *ca*. 140 and 280 K) for all samples when compared with the first order transition observed for powder samples (see ref. 10) or for films assembled on gold surfaces (see ref. 17). The transition is virtually complete at high temperatures, which can be inferred from the complete bleaching of the LS absorption bands. On the other hand, it remains difficult to establish the existence of any residual HS fraction at low temperatures due to the lack of characteristic HS absorption bands. The second important finding concerns the fact that no significant differences in the

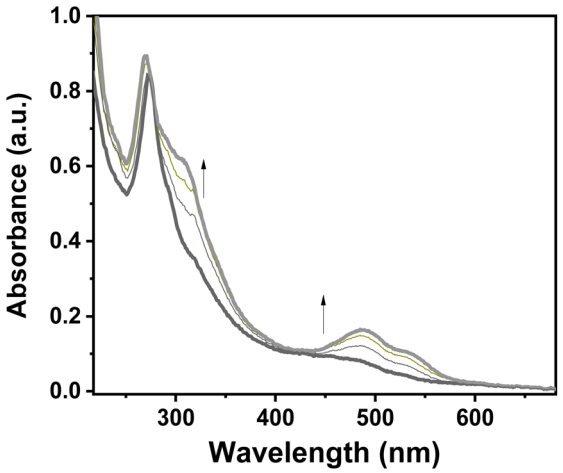

Fig. 2 Evolution of a UV–visible absorption spectra of a **1-Ni** film (N = 50 cycles, T = 293 K, c = 50 mM) recorded upon cooling from 300 K to 100 K.

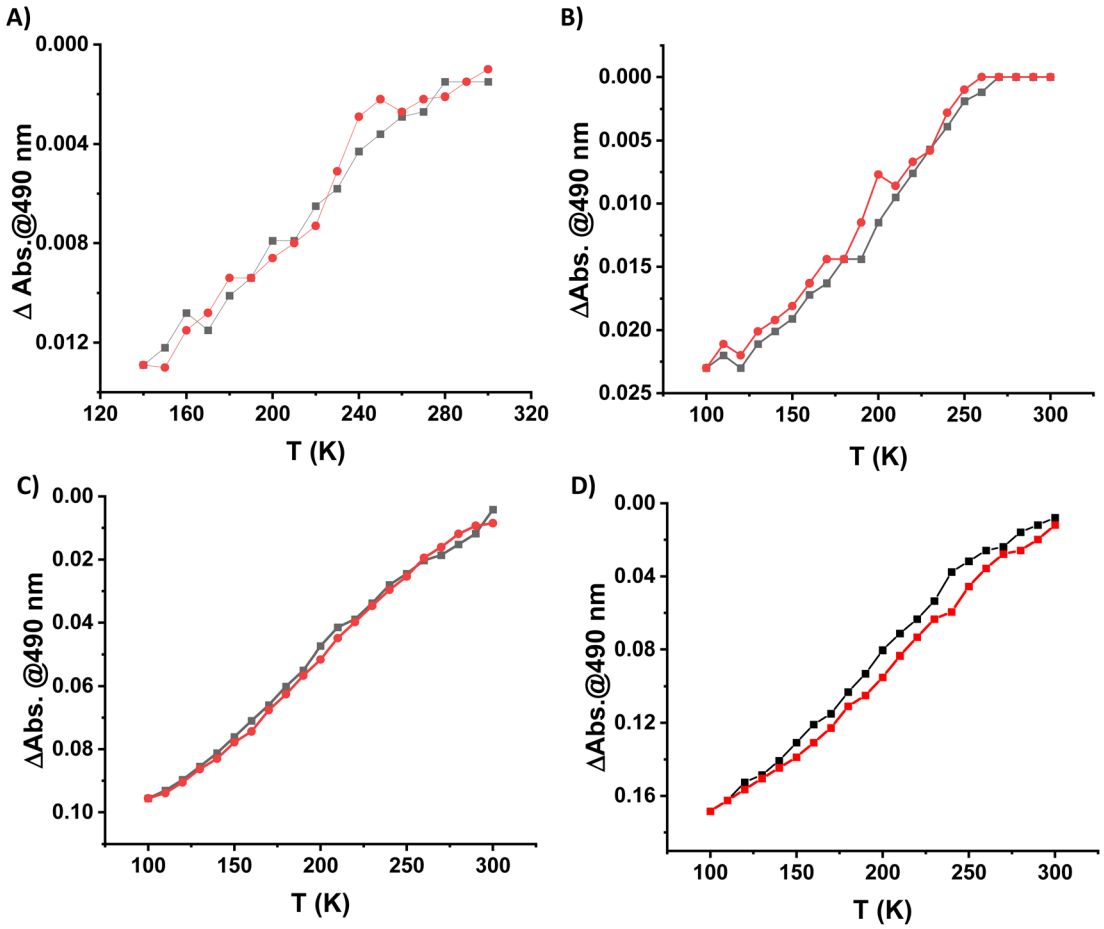

Fig. 3 Temperature dependence of the absorbance band intensity at 490 nm for different films of **1-Ni** deposited at 213 K during 16 deposition cycles using (A) 25 mM, (B) 50 mM, (C) 75 mM and (D) 100 mM reactant concentrations (red: heating processes; black: cooling processes).

SCO properties can be observed when downsizing the film thickness. Again, this finding contrasts with previous reports on thin films deposited on gold surfaces. The most plausible reason for this difference comes from the lack of crystallinity of the films deposited on FS, when compared to the crystalline and quasi-epitaxial films deposited on gold.

In general, it has been already demonstrated in the literature that the corresponding $\{Fe(pz)[\mu_4\text{-}M(CN)_4]\}$ platinum compound as powder[10] or as thin film on gold surfaces[17] presents more abrupt SCO when compared to the nickel analogue and the transition is shifted towards room temperature. With this idea in mind, the Pt derivative has been deposited on a FS

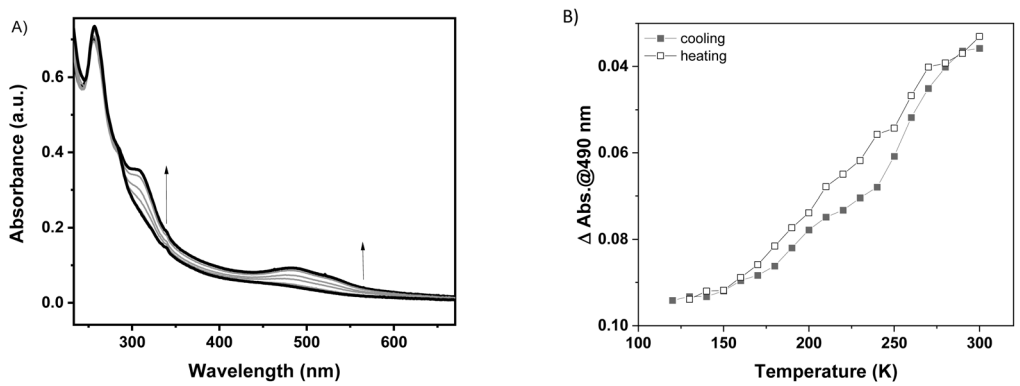

Fig. 4 (A) Evolution of the UV–visible absorption spectra of a **1-Pt** film (N = 20 cycles, T = 253 K, c = 50 mM) recorded upon cooling from 300 K to 100 K. (B) Temperature dependence of the absorbance band intensity at 490 nm.

surface at 253 K over 20 cycles using the same methodology as previously described. The **1-Pt** film was characterized using XRD (see Fig. S14†), which revealed that the **1-Pt** compound is also amorphous, confirming our hypothesis that the starting anchoring layer does not favour the growth of crystalline phases of the compounds. The SCO properties of **1-Pt** have been studied using UV-visible spectroscopy. As shown in Fig. 4, upon cooling, one can observe the emergence of bands located at 307, 490 and 540 nm, which corresponds to the HS → LS transition. Evolution of absorption intensity at 490 nm during the cooling and heating modes, between *ca*. 120 and 300 K, is represented in Fig. 4B. It reveals for the **1-Pt** film a gradual spin crossover, similar to those observed in **1-Ni** films, confirming that the lack of the crystallinity may be considered as a critical point in order to obtain more abrupt SCO.

4. Conclusions

In summary, we have described the successful sequential deposition of the 3D Hofmann clathrate derivatives {Fe(pz)[μ_4-M(CN)$_4$]} on fused silica surfaces, pre-functionalized by 4-pyridinecarboxylic acid. The investigation of deposition conditions by AFM, XRD and spectrophotometry revealed a non-epitaxial growth, deviating from a layer-by-layer scheme. Moreover, it has been shown, that the thin film can be also synthesised at room temperature. Using variable temperature UV-vis spectroscopy, we clearly demonstrate the occurrence of SCO in the films. Importantly, the SCO phenomenon in the films appears very gradual for both the Ni and Pt derivatives and virtually independent of the film thickness, which we attribute to the lack of crystallinity. This capability to deposit such SCO thin films on optically transparent and/or electrically insulating substrates paves the way to applications in electronics or photonics. Work is currently in progress in our laboratory to tune the SCO of the Pt compound above room temperature using oxidative adsorption of iodine molecules as well as to improve the crystallinity of the films in order to get sharper spin transitions.

Conflicts of interest

There are no conflicts of interest to declare.

Acknowledgements

FL thanks the China Scholarship Council for a PhD grant. SC thanks the University of Toulouse III for the "Chaire Professeur Junior" and the Danube program of the Ministry of Foreign Affairs.

References

1 V. F. Yusuf, N. I. Malek and S. K. Kailasa, Review on Metal–Organic Framework Classification, Synthetic Approaches, and Influencing Factors: Applications in Energy, Drug Delivery, and Wastewater Treatment, *ACS Omega*, 2022, **7**(49), 44507–44531, DOI: **10.1021/acsomega.2c05310**.

2 A. E. Baumann, D. A. Burns, B. Liu and V. S. Thoi, Metal-Organic Framework Functionalization and Design Strategies for Advanced Electrochemical Energy Storage Devices, *Commun. Chem.*, 2019, **2**(1), 1–14, DOI: **10.1038/s42004-019-0184-6**.

3 M. C. Muñoz and J. A. Real, Thermo-, Piezo-, Photo- and Chemo-Switchable Spin Crossover Iron(II)-Metallocyanate Based Coordination Polymers, *Coord. Chem. Rev.*, 2011, **255**(17), 2068–2093, DOI: **10.1016/j.ccr.2011.02.004**.

4 Z.-P. Ni, J.-L. Liu, M. N. Hoque, W. Liu, J.-Y. Li, Y.-C. Chen and M.-L. Tong, Recent Advances in Guest Effects on Spin-Crossover Behavior in Hofmann-Type Metal-Organic Frameworks, *Coord. Chem. Rev.*, 2017, **335**, 28–43, DOI: **10.1016/j.ccr.2016.12.002**.

5 K. Otsubo, T. Haraguchi and H. Kitagawa, Nanoscale Crystalline Architectures of Hofmann-Type Metal–Organic Frameworks, *Coord. Chem. Rev.*, 2017, **346**, 123–138, DOI: **10.1016/j.ccr.2017.03.022**.

6 T. Kitazawa, Y. Gomi, M. Takahashi, M. Takeda, M. Enomoto, A. Miyazaki and T. Enoki, Spin-Crossover Behaviour of the Coordination Polymer FeII(C5H5N)2NiII(CN)4, *J. Mater. Chem.*, 1996, **6**(1), 119–121, DOI: **10.1039/JM9960600119**.

7 G. Molnár, V. Niel, J.-A. Real, L. Dubrovinsky, A. Bousseksou and J. J. McGarvey, Raman Spectroscopic Study of Pressure Effects on the Spin-Crossover Coordination Polymers Fe(Pyrazine)[M(CN)4]·2H_2O (M = Ni, Pd, Pt). First Observation of a Piezo-Hysteresis Loop at Room Temperature, *J. Phys. Chem. B*, 2003, **107**(14), 3149–3155, DOI: **10.1021/jp027550z**.

8 S. Bonhommeau, G. Molnár, A. Galet, A. Zwick, J.-A. Real, J. J. McGarvey and A. Bousseksou, One Shot Laser Pulse Induced Reversible Spin Transition in the Spin-Crossover Complex [Fe($C_4H_4N_2$)Pt(CN)4] at Room Temperature, *Angew. Chem., Int. Ed.*, 2005, **44**(26), 4069–4073, DOI: **10.1002/anie.200500717**.

9 M. Ohba, K. Yoneda, G. Agustí, M. C. Muñoz, A. B. Gaspar, J. A. Real, M. Yamasaki, H. Ando, Y. Nakao, S. Sakaki and S. Kitagawa, Bidirectional Chemo-Switching of Spin State in a Microporous Framework, *Angew. Chem., Int. Ed.*, 2009, **48**(26), 4767–4771, DOI: **10.1002/anie.200806039**.

10 V. Niel, J. M. Martinez-Agudo, M. C. Muñoz, A. B. Gaspar and J. A. Real, Cooperative Spin Crossover Behavior in Cyanide-Bridged Fe(II)–M(II) Bimetallic 3D Hofmann-like Networks (M = Ni, Pd, and Pt), *Inorg. Chem.*, 2001, **40**(16), 3838–3839, DOI: **10.1021/ic010259y**.

11 S. Cobo, D. Ostrovskii, S. Bonhommeau, L. Vendier, G. Molnár, L. Salmon, K. Tanaka and A. Bousseksou, Single-Laser-Shot-Induced Complete Bidirectional Spin

Transition at Room Temperature in Single Crystals of (FeII(Pyrazine)(Pt(CN)4)), *J. Am. Chem. Soc.*, 2008, **130**(28), 9019–9024, DOI: 10.1021/ja800878f.

12 S. Sakaida, K. Otsubo, O. Sakata, C. Song, A. Fujiwara, M. Takata and H. Kitagawa, Crystalline Coordination Framework Endowed with Dynamic Gate-Opening Behaviour by Being Downsized to a Thin Film, *Nat. Chem.*, 2016, **8**(4), 377–383, DOI: 10.1038/nchem.2469.

13 A. Bousseksou, G. Molnár, L. Salmon and W. Nicolazzi, Molecular Spin Crossover Phenomenon: Recent Achievements and Prospects, *Chem. Soc. Rev.*, 2011, **40**(6), 3313–3335, DOI: 10.1039/C1CS15042A.

14 T. Mallah and M. Cavallini, Surfaces, Thin Films and Patterning of Spin Crossover Compounds, *C. R. Chim.*, 2018, **21**(12), 1270–1286, DOI: 10.1016/j.crci.2018.02.007.

15 G. Molnár, S. Rat, L. Salmon, W. Nicolazzi and A. Bousseksou, Spin Crossover Nanomaterials: From Fundamental Concepts to Devices, *Adv. Mater.*, 2018, **30**(5), 1703862, DOI: 10.1002/adma.201703862.

16 C. M. Bell, M. F. Arendt, L. Gomez, R. H. Schmehl and T. E. Mallouk, Growth of Lamellar Hofmann Clathrate Films by Sequential Ligand Exchange Reactions: Assembling a Coordination Solid One Layer at a Time, *J. Am. Chem. Soc.*, 1994, **116**(18), 8374–8375, DOI: 10.1021/ja00097a058.

17 S. Cobo, G. Molnár, J. A. Real and A. Bousseksou, Multilayer Sequential Assembly of Thin Films That Display Room-Temperature Spin Crossover with Hysteresis, *Angew. Chem., Int. Ed.*, 2006, **45**(35), 5786–5789, DOI: 10.1002/anie.200601885.

18 G. Agustí, S. Cobo, A. B. Gaspar, G. Molnár, N. O. Moussa, P.Á Szilágyi, V. Pálfi, C. Vieu, M. Carmen Muñoz, J. A. Real and A. Bousseksou, Thermal and Light-Induced Spin Crossover Phenomena in New 3D Hofmann-Like Microporous Metalorganic Frameworks Produced As Bulk Materials and Nanopatterned Thin Films, *Chem. Mater.*, 2008, **20**(21), 6721–6732, DOI: 10.1021/cm8019878.

19 C. Bartual-Murgui, A. Akou, L. Salmon, G. Molnár, C. Thibault, J. A. Real and A. Bousseksou, Guest Effect on Nanopatterned Spin-Crossover Thin Films, *Small*, 2011, **7**(23), 3385–3391, DOI: 10.1002/smll.201101089.

20 C. Bartual-Murgui, L. Salmon, A. Akou, C. Thibault, G. Molnár, T. Mahfoud, Z. Sekkat, J. A. Real and A. Bousseksou, High Quality Nano-Patterned Thin Films of the Coordination Compound {Fe(Pyrazine)[Pt(CN)4]} Deposited Layer-by-Layer, *New J. Chem.*, 2011, **35**(10), 2089–2094, DOI: 10.1039/C1NJ20212J.

21 G. Molnár, S. Cobo, J. A. Real, F. Carcenac, E. Daran, C. Vieu and A. Bousseksou, A Combined Top-Down/Bottom-Up Approach for the Nanoscale Patterning of Spin-Crossover Coordination Polymers, *Adv. Mater.*, 2007, **19**(16), 2163–2167, DOI: 10.1002/adma.200700448.

22 A. Akou, C. Bartual-Murgui, K. Abdul-Kader, M. Lopes, G. Molnár, C. Thibault, C. Vieu, L. Salmon and A. Bousseksou, Photonic Gratings of the Metal–Organic Framework {Fe(Bpac)[Pt(CN)4]} with Synergetic Spin Transition and Host–Guest Properties, *Dalton Trans.*, 2013, **42**(45), 16021–16028, DOI: 10.1039/C3DT51687C.

23 C. Bartual-Murgui, A. Akou, C. Thibault, G. Molnár, C. Vieu, L. Salmon and A. Bousseksou, Spin-Crossover Metal–Organic Frameworks: Promising Materials for Designing Gas Sensors, *J. Mater. Chem. C*, 2015, **3**(6), 1277–1285, DOI: 10.1039/C4TC02441A.

24 K. Otsubo, T. Haraguchi, O. Sakata, A. Fujiwara and H. Kitagawa, Step-by-Step Fabrication of a Highly Oriented Crystalline Three-Dimensional Pillared-Layer-Type Metal–Organic Framework Thin Film Confirmed by Synchrotron X-Ray Diffraction, *J. Am. Chem. Soc.*, 2012, **134**(23), 9605–9608, DOI: 10.1021/ja304361v.

25 S. Sakaida, T. Haraguchi, K. Otsubo, O. Sakata, A. Fujiwara and H. Kitagawa, Fabrication and Structural Characterization of an Ultrathin Film of a Two-Dimensional-Layered Metal–Organic Framework, {Fe(Py) 2 [Ni(CN) 4]} (Py = Pyridine), *Inorg. Chem.*, 2017, **56**(14), 7606–7609, DOI: 10.1021/acs.inorgchem.7b01113.

26 S. Sakaida, K. Otsubo, K. Otake, S. Kawaguchi, M. Maesato, S. Kitagawa and H. Kitagawa, Surface Morphology-Induced Spin-Crossover-Inactive High-Spin State in a Coordination Framework, *Chem. Commun.*, 2021, **57**(12), 1462–1465, DOI: 10.1039/D0CC06682F.

27 S. Sakaida, K. Otsubo, M. Maesato and H. Kitagawa, Crystal Size Effect on the Spin-Crossover Behavior of {Fe(Py)2[Pt(CN)4]} (Py = Pyridine) Monitored by Raman Spectroscopy, *Inorg. Chem.*, 2020, **59**(23), 16819–16823, DOI: 10.1021/acs.inorgchem.0c02874.

28 T. Haraguchi, K. Otsubo, O. Sakata, A. Fujiwara and H. Kitagawa, Strain-Controlled Spin Transition in Heterostructured Metal–Organic Framework Thin Film, *J. Am. Chem. Soc.*, 2021, **143**(39), 16128–16135, DOI: 10.1021/jacs.1c06662.

29 V. Rubio-Giménez, C. Bartual-Murgui, M. Galbiati, A. Núñez-López, J. Castells-Gil, B. Quinard, P. Seneor, E. Otero, P. Ohresser, A. Cantarero, E. Coronado, J. A. Real, R. Mattana, S. Tatay and C. Martí-Gastaldo, Effect of Nanostructuration on the Spin Crossover Transition in Crystalline Ultrathin Films, *Chem. Sci.*, 2019, **10**(14), 4038–4047, DOI: 10.1039/C8SC04935A.

30 C. Bartual-Murgui, V. Rubio-Giménez, M. Meneses-Sánchez, F. J. Valverde-Muñoz, S. Tatay, C. Martí-Gastaldo, M. C. Muñoz and J. A. Real, Epitaxial Thin-Film vs Single Crystal Growth of 2D Hofmann-Type Iron(II) Materials: A Comparative Assessment of Their Bi-Stable Spin Crossover Properties, *ACS Appl. Mater. Interfaces*, 2020, **12**(26), 29461–29472, DOI: 10.1021/acsami.0c05733.

31 V. Rubio-Giménez, G. Escorcia-Ariza, C. Bartual-Murgui, C. Sternemann, M. Galbiati, J. Castells-Gil, J. A. Real, S. Tatay and C. Martí-Gastaldo, Ultrathin Films of 2D Hofmann-Type Coordination Polymers: Influence of Pillaring Linkers on Structural Flexibility and Vertical Charge Transport, *Chem. Mater.*, 2019, **31**(18), 7277–7287, DOI: 10.1021/acs.chemmater.9b01634.

32 A. Núñez-López, R. Torres-Cavanillas, M. Morant-Giner, N. Vassilyeva, R. Mattana, S. Tatay, P. Ohresser, E. Otero,

E. Fonda, M. Paulus, V. Rubio-Giménez, A. Forment-Aliaga and E. Coronado, Hybrid Heterostructures of a Spin Crossover Coordination Polymer on MoS_2: Elucidating the Role of the 2D Substrate, *Small*, 2023, **19**(50), 2304954, DOI: **10.1002/smll.202304954**.

33 S. P. Pujari, L. Scheres, A. T. M. Marcelis and H. Zuilhof, Covalent Surface Modification of Oxide Surfaces, *Angew. Chem., Int. Ed.*, 2014, **53**(25), 6322–6356, DOI: **10.1002/anie.201306709**.

34 W. R. I. Mason and H. B. Gray, Electronic Structures of Square-Planar Complexes, *J. Am. Chem. Soc.*, 1968, **90**(21), 5721–5729, DOI: **10.1021/ja01023a012**.

35 J. J. Stapleton, D. L. Suchy, J. Banerjee, K. T. Mueller and C. G. Pantano, Adsorption Reactions of Carboxylic Acid Functional Groups on Sodium Aluminoborosilicate Glass Fiber Surfaces, *ACS Appl. Mater. Interfaces*, 2010, **2**(11), 3303–3309, DOI: **10.1021/am100730z**.

36 P. D. Southon, L. Liu, E. A. Fellows, D. J. Price, G. J. Halder, K. W. Chapman, B. Moubaraki, K. S. Murray, J.-F. Létard and C. J. Kepert, Dynamic Interplay between Spin-Crossover and Host–Guest Function in a Nanoporous Metal–Organic Framework Material, *J. Am. Chem. Soc.*, 2009, **131**(31), 10998–11009, DOI: **10.1021/ja902187d**.

37 K. H. Lam, T. R. B. Foong, J. Zhang, A. C. Grimsdale and Y. M. Lam, Carboxylic Acid Mediated Self-Assembly of Small Molecules for Organic Thin Film Transistors, *Org. Electron.*, 2014, **15**(7), 1592–1597, DOI: **10.1016/j.orgel.2014.03.041**.

38 G. Félix, W. Nicolazzi, L. Salmon, G. Molnár, M. Perrier, G. Maurin, J. Larionova, J. Long, Y. Guari and A. Bousseksou, Enhanced Cooperative Interactions at the Nanoscale in Spin-Crossover Materials with a First-Order Phase Transition, *Phys. Rev. Lett.*, 2013, **110**(23), 235701, DOI: **10.1103/PhysRevLett.110.235701**.